COMMUNICATION

Check for updates

Buckling in armored droplets†

François Sicard ID * and Alberto Striolo ID

The buckling mechanism in droplets stabilized by solid particles (armored droplets) is tackled at a mesoscopic level using dissipative particle dynamics simulations. We consider one spherical water droplet in a decane solvent coated with nanoparticle monolayers of two different types: Janus (particles whose surface shows two regions with different wetting properties) and homogeneous. The chosen particles yield comparable initial three-phase contact angles, selected to maximize the adsorption energy at the interface. We study the interplay between the evolution of droplet shape, layering of the particles, and their distribution at the interface when the volume of the droplets is reduced. We show that Janus particles affect strongly the shape of the droplet with the formation of a crater-like depression. This evolution is actively controlled by a close-packed particle monolayer at the curved interface. In contrast, homogeneous particles follow passively the volume reduction of the droplet, whose shape does not deviate too much from spherical, even when a nanoparticle monolayer/bilayer transition is detected at the interface. We discuss how these buckled armored droplets might be of relevance in various applications including potential drug delivery systems and biomimetic design of functional surfaces.

Pickering emulsions,[1] *i.e.* particle-stabilized emulsions, have been studied intensively in recent years owing to their wide range of applications including biofuel processing[2] and food preservation.[3,4] They have also been developed as precursors to magnetic particles for imaging[5] and drug delivery systems.[6] Even with their widespread use, they remain, however, under-utilized. In Pickering emulsions, particles and/or nano-particles (NPs) with suitable surface chemistries adsorb at the droplet surfaces, with adsorption energy of up to thousands of times the thermal energy. The characteristics of Pickering emulsions pose a number of intriguing fundamental physical questions including a thorough understanding of the peren-

nial lack of detail about how particles arrange at the liquid/liquid interface. Other not completely answered questions include particle effects on interfacial tension,[7] layering,[8] buckling[9–11] and particle release.[8,12]

In some important processes that involve emulsions, it may be necessary to reduce the volume of the dispersed droplets.[9,13–15] The interface may undergo large deformations that produce compressive stresses, causing localized mechanical instabilities. The proliferation of these localized instabilities may then result in a variety of collapse mechanisms.[8,10,11] Despite the vast interest in particle-laden interfaces, the key factors that determine the collapse of curved particle-laden interfaces are still a subject of debate. Indeed, although linear elasticity describes successfully the morphology of buckled particle-laden droplets, it is still unclear whether the onset of buckling can be explained in terms of classic elastic buckling criteria,[16,17] capillary pressure-driven phase transition,[9] or interfacial compression phase transition.[18] Numerous experiments have been conducted to link the rheological response of particle-laden interfaces to the stability of emulsions and foams. However, their results could be dependent on the method chosen for preparing the interfacial layer. Due to their inherent limited resolution, direct access to local observables, such as the particles' three-phase contact angle distribution, remains out of reach.[19] This crucial information can be accessed by numerical simulations sometimes with approximations. All-atom molecular dynamics (MD) simulations have become a widely employed computational technique. However, all-atom MD simulations are computationally expensive. Moreover, most phenomena of interest here take place on time scales that are orders of magnitude longer than those accessible *via* all-atom MD. Mesoscopic simulations, in which the structural unit is a coarse-grained representation of a large number of molecules, allow us to overcome these limitations. It is now well established that coarse-grained approaches offer the possibility of answering fundamental questions responsible for the collective behaviour of particles anchored at an interface.[20] Analytical models have also been proposed to study the thermodynamic properties of colloidal particles at

Department of Chemical Engineering, University College London, Torrington Place, London WC1E 7JE, UK. E-mail: francois.sicard@free.fr
†Electronic supplementary information (ESI) available. See DOI: 10.1039/C7NR01911D

the fluid interface upon the deformation of a spherical droplet.[21–23] However, these studies were limited to a pair of particles and small deformations, and did not take into account the particles' collective dynamics.

We employ here Dissipative Particle Dynamics (DPD)[24] as a mesoscopic simulation method. We study the shape and buckling transitions of model water droplets coated with spherical nanoparticles and immersed in an organic solvent. The procedure and the parameterisation details are fully described in prior work[25–27] and in the ESI.† The particles are of two different types: Janus and homogeneous. They are chosen so that the initial three-phase contact angles ($\approx 90°$) result in maximum adsorption energy. The volume of the droplets is systematically reduced, by pumping a constant proportion of water molecules out of the droplet (more details in the ESI†). At every stage we remove 10 percent of the water from the current droplet configuration. Throughout this letter, E_i refers to the ith removal of water, with E_0 corresponding to the initial configuration and E_{20} to the final configuration. E_1 corresponds to a water droplet with 90% of the initial water content, and E_{20} to a water droplet containing only 16% of the initial water content. We seek to determine whether the NPs at the droplet interface buckle, causing the droplets to deviate from the spherical shape. We show that Janus particles affect strongly the shape of the droplet *via* the formation of a crater-like depression. This evolution is actively controlled by a close-packed particle monolayer at the curved interface. On the other hand, homogeneous particles follow passively the volume reduction of the droplet. The shape of the droplet remains approximately spherical with a nanoparticle monolayer/bilayer transition, with some NPs desorbing in water. We discriminate the two mechanisms with the evolution of their respective nanoparticle three-phase contact angle distributions. While for Janus particles the distribution remains unimodal, albeit skewed when the droplet significantly shrinks, for homogeneous particles, the evolution of the contact angle distribution becomes bimodal with some particles becoming more/less immersed in the aqueous phase.

We consider a system initially made by a spherical water droplet immersed in oil, and stabilized by a sufficiently dense layer of NPs.[27] The initial shape of the droplet is spherical. The only difference between the two systems is the NP chemistry, *i.e.* the distribution and proportion of polar and apolar beads around the spherical particles and their efficiency in interacting with the two fluids at the interface. Janus and homogeneous NPs are designed to present comparable three-phase contact angles, $\theta_c = (91.6 \pm 2.0)°$ and $\theta_c = (88.7 \pm 3.5)°$, respectively (*cf.* the ESI† for details). We consider throughout this study the same NP density on the droplets. We calculate the radius of gyration, R_{GYR}, and the asphericity, A_s, for the droplet covered by either Janus or homogeneous NPs (*cf.* ESI† for details). For the initial configurations, we obtain $R_{GYR} = 13.837 \pm 0.003$ and $R_{GYR} = 13.860 \pm 0.003$, and $A_s = 0.156 \pm 0.05$ and $A_s = 0.153 \pm 0.05$, respectively, expressed in R_C units (*cf.* ESI† for details).

In Fig. 1 we show representative snapshots obtained during the simulations for systems containing Janus NPs (top panels) and homogeneous NPs (bottom panels). Visual inspection of the simulation snapshots highlights some fundamental differences between the two buckling processes. We start with spherical initial droplets (E_0). When the water droplet is coated with Janus particles (top), the system starts developing dimples as a moderate amount of water is removed (E_2). The morphology then becomes more crumpled with an increasing number of dimples (E_5). For stronger removal, the droplet geometry evolves to a large and smooth curved shape, yielding a crater-like depression to minimize the interfacial energy of the system (E_8 and E_{20}). During this evolution, Janus NPs remain strongly adsorbed at the interface, forming a close-packed monolayer between the two fluids.

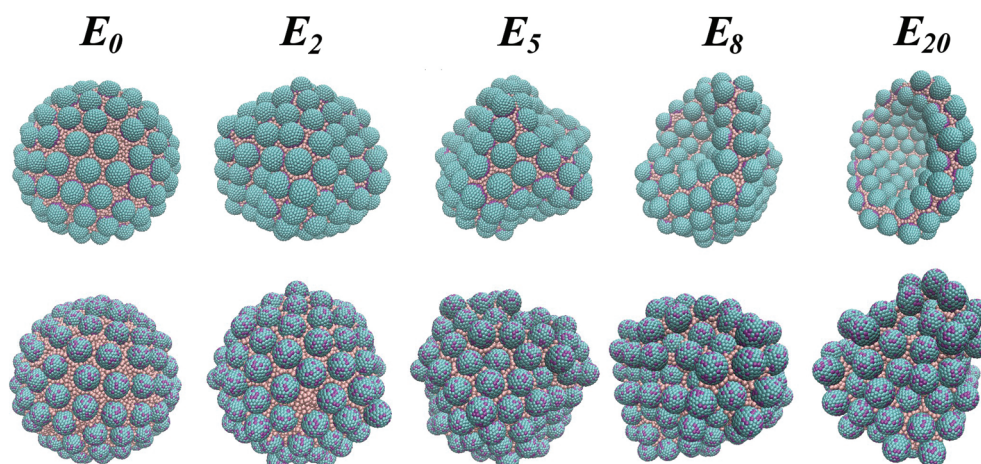E_0 E_2 E_5 E_8 E_{20}

Fig. 1 Sequence of simulation snapshots representing buckling processes of water in oil droplets armored with 160 spherical Janus (top) and homogeneous (bottom) nanoparticles after successive removals of water. The number of water beads removed increases from left to right with E_i referring to the ith removal. Cyan and purple spheres represent polar and apolar beads, respectively. Pink spheres represent water beads. The oil molecules surrounding the system are not shown for clarity.

The buckling process is fundamentally different when the water droplet is stabilized with homogeneous NPs (bottom). When the volume of the droplet is reduced, the shape of the system evolves smoothly and does not present any sharp transitions to morphologies showing dimples and cups, nor crater-like depressions. Instead, the NPs reorganize progressively into a bilayer, presumably to minimize the system energy. Unlike Janus NPs, homogeneous NPs either protrude exceedingly towards the decane solvent, or recede into the water droplet with some particles even desorbing into the water phase (from E_2 to E_{20}). For reference, we recall that the change in energy accompanying desorption of a spherical particle from the oil–water interface to either bulk phase is approximated by $\Delta E = \pi r^2 \gamma_{ow}(1 \pm \cos\theta)^2$, in which r is the particle radius, γ_{ow} is the bare oil–water interfacial tension, and the plus(minus) sign refers to desorption into oil (water).[19] Even if this expression assumes that the oil–water interface remains planar up to the contact line with the particle, it can give a rough approximation of the energy at play. Considering the system parameters given in the ESI,† we obtain $\Delta E \approx 85 k_B T$ in our systems when one NP desorbs.

These two different behaviours are quantitatively investigated as shown in Fig. 2, where we show the temporal evolution of the radius of gyration (left panel), R_{GYR}, and the asphericity (right panel), A_s, of the two droplets as a function of the dimensionless parameter $\Delta N_W \equiv N_W/N_W^0$, where N_W is the number of water beads remaining in the droplet, and N_W^0 is the initial number of water beads in the droplet. When $N_W > 0.6$, the radius of gyration of two systems follows the same evolution, regardless the chemistry of the NPs (Janus or homogeneous). For one droplet coated with Janus NPs, R_{GYR} then departs from its linear trend when $N_W < 0.6$. This departure corresponds to the evolution from E_5 to E_8 in Fig. 1, *i.e.* the transition from a droplet interface made of dimples and cups to the formation of the crater-like depression. During this transition, the size of one dimple increases when the system relaxes after evaporation. This local evolution yields a larger depression, which causes the progressive coalescence of the small dimples. This transition is consistent with the surface model numerical analysis reported by Quilliet,[17] which studies the shape evolution of a spherical elastic surface when the volume it encloses is decreased. This model, which has long been considered as valid to describe the deformation of thin shells,[16,28] showed that a thin shell with a single dimple has lower energy than a shell containing multiple dimples. This occurs because elastic energy mainly concentrates in dimple edges as bending energy.[29,30] Dimple coalescence lowers the total elastic energy. Below $\Delta N_W \approx 0.6$, R_{GYR} increases as the droplet can be described as half-sphered. Let us note that this evolution is coherent with the temporal evolution of the radial distribution function of the NPs, $g(r)$, with r the distance between the centers of the NPs, given in the ESI.† In contrast, the droplet coated with homogeneous NPs shrinks isotropically when the volume reduces even below $\Delta N_W \approx 0.6$. This evolution yields continuous decrease of R_{GYR} and a relatively low A_s as shown in Fig. 2. Eventually, the NP concentration becomes too high and some NPs move into the droplet. When $N_W < 0.25$, the number of water beads that remain in the droplet is not sufficient to define unambiguously the droplet volume. This limitation impacts the system shape and the evolution of R_{GYR} and A_s for Janus and homogeneous NPs.

We also quantify the NP layer properties as a function of the particle three-phase contact angle distribution. In Fig. 3, we compare the three phase contact angle distribution of Janus (left panel) and homogeneous (right panel) NPs at the initial stage E_0, where the shape of the droplet is spherical, and the final stage, E_{20}. The initial distributions, fitted with continuous lines, can be described with Gaussian distributions for both NPs. The values of the respective means, μ^J and μ^H, and variances, σ^J and σ^H, differ due to the NP chemistry. We obtain $\mu^J = 91.6°$ and $\mu^H = 88.6°$, and $\sigma^J = 2.0°$ and $\sigma^J = 3.4°$ for Janus and homogeneous NPs, respectively. When the droplet coated with Janus NPs shrinks, the contact angle distribution evolves to a skewed one, but it remains unimodal, with a single peak centered at the same value as the one measured for the initial configuration. The emergence of the skewness of the distribution is linked to the decrease of the NP–NP distance when the droplet volume is reduced. It is due to the major role played by steric effects. As discussed earlier, to minimize its interfacial energy, the system must deform its shape, eventually forming a crater-like depression. We conclude this transition is achieved through the active role played by the Janus NPs due to the strong adhesion of the Janus NPs, compared with the homogenous NPs, to the interface,[31] and possibly to the restricted rotational freedom of Janus *vs.* homogeneous NPs.[32] In the final structure, some NPs are forced to deviate from their original contact angle, increasing the skewness of the distribution on both sides of the peak.

The evolution of the system is different when homogeneous NPs are present. As the droplet volume is reduced, the contact angle distribution firstly evolves as a monolayer interface with a single peak (*cf.* the ESI†). As the droplet shrinks further, and the distance between the NPs decreases, the distribution becomes bimodal, with two distinct peaks emerging on both
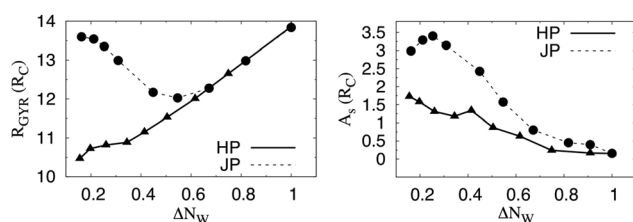

Fig. 2 Temporal evolution of the radius of gyration, R_{GYR} (left panel) and the asphericity A_s (right panel), for armored droplets stabilized with Janus (circles and dashed line) and homogeneous NPs (triangles and plain line) as a function of the dimensionless parameter $\Delta N_W \equiv N_W/N_W^0$. N_W represents the number of water beads that remain in the droplet after each removal, and N_W^0 is the initial number of water beads. The statistical errors are estimated as one standard deviation from the average obtained for equilibrated trajectories, and they are always smaller than the symbols. For comparison with snapshots in Fig. 1, $\Delta N_W(E_2) \approx 0.82$, $\Delta N_W(E_5) \approx 0.62$, $\Delta N_W(E_8) \approx 0.45$, and $\Delta N_W(E_{20}) \approx 0.16$.
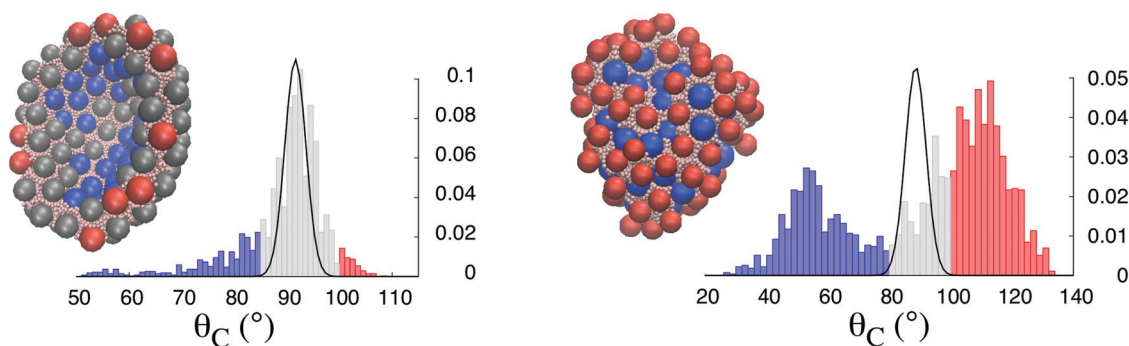
Fig. 3 Three-phase contact angle distribution of Janus (left panel) and homogeneous (right panel) NPs at the initial stage E_0 (continuous black lines) where the shape of the droplet is spherical, and at the final stage E_{20} (histograms). The initial distributions (stage E_0) are fitted with Gaussian distributions for both systems. The droplet configurations at the final stage E_{20} are also shown. The blue, gray, and red spheres represent the NPs with three-phase contact angles in the three respective regions highlighted in the histogram distributions.

sides of the initial equilibrium contact angle. This feature is characteristic of a particle bilayer. Indeed, homogeneous NPs are more weakly attached to the interface than Janus NPs, with some large degree of rotational freedom.[32] In the case of the buckling mechanism studied here, the homogenous NPs mainly follow the volume reduction, sharing the interfacial area, either receding into the water droplet or protruding towards the organic solvent. Unlike Janus NPs, homogeneous NPs do not drive the evolution of the droplet shape, which does not differ too much from the spherical geometry. The behaviour just described is characteristic of the passive role played by the homogeneous NPs, which mainly follows the volume reduction, only modulating the droplet shape due to the steric constraints.

The curved shape obtained when the droplet is coated with Janus NPs can also be characterized by the wettability associated with the local arrangement of the NPs at the interface. The particles with a contact angle $\theta_c < 85°$, *i.e.* the blue ones in Fig. 3 (left panel), can be found in the crater-like depression. These particles have receded into the water droplet due to the concave local geometry of the interface. The particles with $\theta_c > 100°$, *i.e.* the red ones in Fig. 3 (left panel), can be found at the transition between the concave and convex areas of the interface, where they are likely to protrude towards the solvent. The shape deformation of the droplet is achieved through the

active role played by the Janus NPs. Their specific chemistry causes them to create an interface with excess wettability ($\theta_c < 85°$) in a pocket delimited by the crater-like depression, and surrounded by a cup with low wettability ($\theta_c > 100°$).

Our results are consistent with experiments reporting buckling and crumpling of nanoparticle-coated droplets.[9–11] In particular, we observe a close analogy to the experimental work of Datta *et al.*,[11] who studied water-in-oil droplets of varying sizes. In these experiments the dispersed phase is slightly soluble in the continuous phase. The volume reduction was controlled with the addition of a fixed amount of the unsaturated continuous phase. As shown in Fig. 4, Datta *et al.* observed droplet shapes including dimples, cups, and folded configurations, in agreement with our simulations (*cf.* experimental details in the caption of Fig. 4). Unlike our mesoscopic analysis, Datta *et al.*[11] do not have access to the particle three-phase contact angle distribution. This information provides a deeper understanding of the organisation of the NPs at the interface, and allows us to decipher the active or passive role of the NPs. The simulations discussed here artificially remove water from the interior of the droplet at a desired rate. The process is meant to mimic the response of the droplet to changes in the water chemical potential within the organic solvent. To obtain a closer connection with the experiments, it would be desirable to compute the water chemical potential
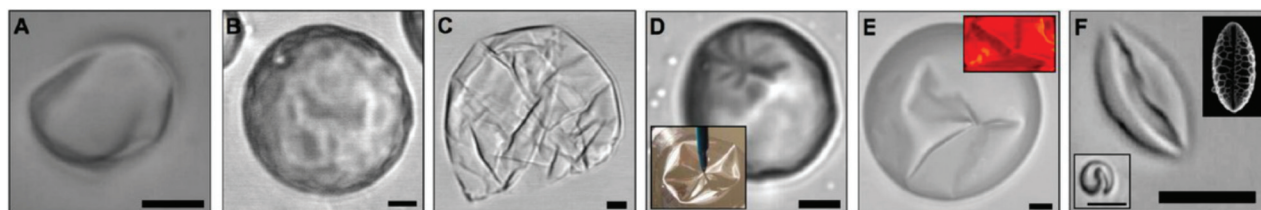

Fig. 4 Optical micrographs of buckled droplets obtained experimentally by Datta *et al.*[11] Panels (A–C) show characteristic shapes at increasing levels of evaporation, and panels (D–F) show typical buckled structures (*cf.* ref. 11 for experimental details). All scale bars are 5 μm. Datta *et al.* used hydrophilic silica NPs coated with a diffuse layer of alkane, rendering them partially hydrophobic and partially hydrophilic. The resulting three-phase contact angle in ref. 11 was ≈90°. Reprinted (adapted) with permission from *Langmuir*, 2010, **26**(24), 18612–18616, DOI: 10.1021/la103874z. Copyright 2010 American Chemical Society.

within the droplet during the process described here. However, while the DPD algorithm mimics successfully hydrodynamics properties,[24] in the present implementation it cannot accurately describe the vapour–liquid coexistence of water[33] (see the ESI† for more details). Such details could be obtained reverting to atomistic models.

As explained in the ESI,† the layering properties of the particles depend strongly on the numerical protocol. For example, decreasing the relaxation time between successive water removals can induce NP release from the interface, which is in agreement with experiments.[12] The results presented here seem to be due to the chemistry of the nanoparticles simulated (*i.e.* Janus *vs.* homogeneous). It is however possible that homogeneous NPs with large adsorption energy become active and yield buckled armored droplets similar to those observed when Janus NPs are simulated here.

The new physical insights discussed in this letter could be useful for a variety of applications. For example, controlling the positions of the solid particles with respect to the interface could help in heterogeneous catalysis.[34] In biomimetic design, where the identification and evaluation of surface binding-pockets is crucial, the ability of controlling pockets such as those created by the crater-like depression in the presence of Janus NPs, could play a central role in designing structures with a defined geometry.[35] The analogy between Fig. 1 and the shape of protein active site might play an important role for ligand docking.[36,37] Finally, buckled armored droplets might also be of relevance as potential drug delivery systems.[6] Over the last decade, nanoscale droplets have been used for instant real-time ultrasound imaging of specific organs.[5] Superparamagnetic solid NPs provide a means of manipulating the droplets using an external magnetic field.[5] One of the main limitations in such applications is droplet coalescence, which can happen before droplets reach the target. The specific shapes obtained with buckled armored droplets might prevent coalescence. Indeed, the NP arrangements on the droplets show increased packing, which reduces significantly the NPs' mobility. The particle layers would then provide enough mechanical resistance to guarantee the droplet stability.

References

1 S. Pickering, *J. Chem. Soc.*, 1907, **91**, 2001–2021.
2 S. Drexler, J. Faria, M. Ruiz, J. Harwell and D. Resasco, *Energy Fuels*, 2012, **26**, 2231–2241.
3 E. Shchukina and D. Shchukin, *Curr. Opin. Colloid Interface Sci.*, 2012, **17**, 281–289.
4 C. Puglia and F. Bonina, *Expert Opin. Drug Delivery*, 2012, **9**, 429–441.
5 J. Lee, D. Carugo, C. Crake, J. Owen, M. de Saint Victor, A. Seth, C. Coussios and E. Stride, *Adv. Mater.*, 2015, 5484–5492.
6 J. Frelichowska, M.-A. Bolzinger, J.-P. Valour, H. Mouaziz, J. Pelletier and Y. Chevalier, *Int. J. Pharm.*, 2009, 7–15.
7 R. Miller, V. Fainerman, V. Kovalchuk, D. Grigoriev, M. Leser and M. Michel, *Adv. Colloid Interface Sci.*, 2006, 128–130.
8 S. Razavi, K. Cao, B. Lin, K. Lee and R. Tu, *Langmuir*, 2015, **31**, 7764–7775.
9 N. Tsapis, E. Dufresne, S. Sinha, J. Hutchinson, L. Mahadevan and D. Weitz, *Phys. Rev. Lett.*, 2005, **94**, 018302.
10 H. Xu, S. Melle, K. Golemanov and G. Fuller, *Langmuir*, 2005, **21**, 10016–10020.
11 S. Datta, H. Shum and D. Weitz, *Langmuir Lett.*, 2010, **26**, 18612–18616.
12 V. Garbin, J. Crocker and J. Stebe, *Langmuir*, 2012, **28**, 1663–1667.
13 L. Pauchard, F. Parisse and C. Allain, *Phys. Rev. E: Stat. Phys., Plasmas, Fluids, Relat. Interdiscip. Top.*, 1999, **59**, 3737–3740.
14 Y. Gorand, L. Pauchard, G. Calligari, J. Hullin and C. Allain, *Langmuir*, 2004, **20**, 5138–5140.
15 L. Pauchard and C. Allain, *Europhys. Lett.*, 2003, **62**, 897–903.
16 L. D. Landau, L. Pitaevskii, A. Kosevich and E. Lifshitz, *Theory of elasticity*, Elsevier Butterworth-Heinemann, Oxford, UK, 1986.
17 C. Quilliet, *Eur. Phys. J. E: Soft Matter Biol. Phys..*, 2012, **35**, 48.
18 A. Salmon, R. Parker, A. Groombridge, A. Maestro, R. Coulston, J. Hegemann, J. Kierfeld, O. Scherman and C. Abell, *Langmuir*, 2016, **32**, 10987–10994.
19 B. Binks and D. Yin, *Soft Matter*, 2016, **12**, 6858–6867.
20 A. Clark, M. Lal, J. Ruddock and P. Warren, *Langmuir*, 2000, **16**, 6342–6350.
21 J. Guzowski, M. Tasinkevych and S. Dietrich, *Eur. Phys. J. E*, 2010, **33**, 219–242.
22 J. Guzowski, M. Tasinkevych and S. Dietrich, *Phys. Rev. E: Stat. Phys., Plasmas, Fluids, Relat. Interdiscip. Top.*, 2011, **84**, 031401.
23 J. Guzowski, M. Tasinkevych and S. Dietrich, *Soft Matter*, 2011, **7**, 4189–4197.
24 R. Groot and P. Warren, *J. Chem. Phys.*, 1997, **107**, 4423–4435.
25 X.-C. Luu, J. Yu and A. Striolo, *Langmuir*, 2013, **29**, 7221–7228.
26 X.-C. Luu, J. Yu and A. Striolo, *J. Phys. Chem. B*, 2013, **117**, 13922–13929.
27 F. Sicard and A. Striolo, *Faraday Discuss.*, 2016, **191**, 287–304.
28 B. Audoly and Y. Pomeau, *Elasticity and Geometry: from hair curls to the nonlinear response of shells*, Oxford University Press, Oxford, UK, 2010.

29 F. Quemeneur, C. Quilliet, M. Faivre, A. Viallat and B. Pépin-Donat, *Phys. Rev. Lett.*, 2012, **108**, 108303.

30 F. Boulogne, F. Giorgiutti-Dauphiné and L. Pauchard, *Soft Matter*, 2013, **9**, 750–757.

31 H. Fan, D. Resasco and A. Striolo, *Langmuir*, 2011, **27**, 5264–5274.

32 D. Cheung and S. Bon, *Soft Matter*, 2009, **5**, 3969–3976.

33 P. Warren, *Phys. Rev. E: Stat. Phys., Plasmas, Fluids, Relat. Interdiscip. Top.*, 2003, **68**, 066702.

34 S. Crossley, J. Faria and D. Resasco, *Science*, 2010, **327**, 68–72.

35 A. Patel and S. Garde, *Science*, 2010, **327**, 68–72.

36 M. Weisel, E. Proschak and G. Schneider, *Chem. Cent. J.*, 2007, 1–7.

37 E. Marcos, B. Basanta, T. Chidyausiku, Y. Tang, G. Oberdorfer, G. Liu, G. Swapna, R. Guan, D.-A. Silva, J. Dou, J. Pereira, R. Xiao, B. Sankaran, P. Zwart, G. Montelione and D. Baker, *Science*, 2017, **355**, 201–206.